Sensing transport: label-free in vitro assays as an atTRACTive alternative for solute carrier transporter drug discovery

Sijben, H.J.

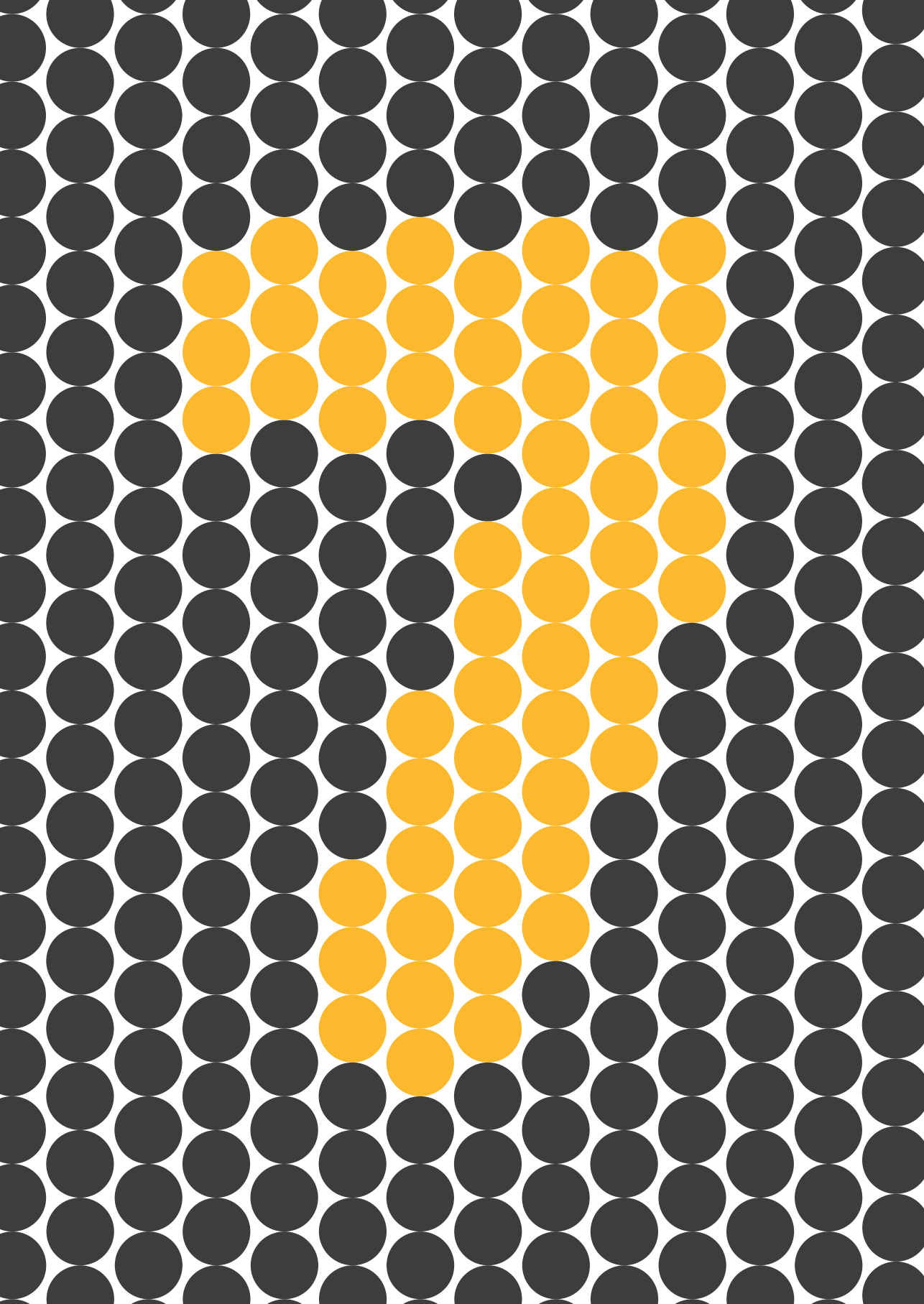

CHAPTER 7

Molecular insights into disease-associated glutamate transporter variants using *in silico* and *in vitro* approaches

Marina Gorostiola González †
Hubert J. Sijben †
Laura Dall' Acqua
Rongfang Liu
Adriaan P. IJzerman
Gerard J.P. van Westen
Laura H. Heitman

Glutamate is an essential excitatory neurotransmitter and an intermediate for energy metabolism. Depending on the tumor site, cancer cells have increased or decreased expression of excitatory amino acid transporter 1 or 2 (EAAT1/2, SLC1A3/2) to regulate glutamate uptake for the benefit of tumor growth. Thus, EAAT1/2 may be an attractive target for therapeutic intervention. Genetic variation of EAAT1 has been associated with rare cases of episodic ataxia, but the occurrence and functional contribution of EAAT1 mutants in other diseases, such as cancer, is poorly understood. In this chapter, we identified 105 unique somatic EAAT1 mutations in cancer patients from the Genomic Data Commons dataset. Using EAAT1 crystal structures and *in silico* simulations, we selected eight mutations based on their close proximity to the orthosteric or allosteric ligand binding sites and the predicted change in ligand binding affinity. *In vitro* functional assessment in the live-cell, impedance-based phenotypic assay described in **Chapter 6** demonstrated that these mutants differentially affect L-glutamate and L-aspartate transport, as well as the inhibitory potency of an orthosteric (TFB-TBOA) and allosteric (UCPH-101) inhibitor. Moreover, two episodic ataxia-related mutants displayed functional responses that were in line with literature, which confirmed the validity of our assay. We demonstrate the application of a robust *in vitro* method to functionally characterize EAAT1 variants, which could substantiate mechanistic studies and aid drug discovery efforts.

Manuscript in preparation
† These authors have contributed equally

7.1 – Introduction

Glutamate is an abundant endogenous amino acid that acts as the major excitatory neurotransmitter in the central nervous system and serves as a key metabolite in energy homeostasis[1]. In the synaptic cleft glutamate is transported across the cell membrane *via* excitatory amino acid transporters (EAATs), which belong to subfamily 1 of the solute carrier (SLC) transporters[2]. Glutamate transport is thermodynamically coupled to the transport of three Na^+ ions and one proton, and the counter-transport of one K^+ ion, where binding of Na^+ and/or substrate activates an uncoupled Cl^- conductive state[3]. Deregulated glutamate levels have been associated with a plethora of neurological diseases[4,5] and more recently with cancer[6,7]. As a result, pharmacological modulation of EAATs may be a promising therapeutic strategy for conditions that are associated with altered glutamate levels[8,9].

Depending on the location of the tumor, cancerous cells have been shown to exploit the uptake, metabolism and signaling properties of glutamate as well as aspartate as fuel for tumor proliferation and a key advantage for expansion. Healthy glia cells abundantly express EAAT1 and EAAT2 to mediate the majority of glutamate clearance[2]. However, expression levels of EAAT2 are vastly reduced in gliomas, which combined with increased efflux *via* the glutamate/cystine antiporter (xCT, SLC7A11) leads to elevated glutamate levels surrounding the glioma that induce cell death and allow further growth of the tumor[10,11]. Moreover, EAAT1 was found to be overexpressed and cause glutamate efflux in aggressive glioblastomas, which indicates selective EAAT1 inhibitors as a potential treatment option for glioma[12]. In several instances of cancer in peripheral tissues EAAT1 expression has been linked to a poor disease prognosis. Under hypoxia or conditions that starve the tumor of glutamine, some cancer cells promote EAAT1 or EAAT2 expression to drive uptake of aspartate or glutamate which rescues cancer cell growth[13–15]. As such, EAAT expression in such tumors could be a predictive biomarker and pharmacological modulation of glutamate transporter expression or activity could be of therapeutic interest.

Despite the clear advantages for tumor cells to regulate EAAT expression, little is known about human genetic variations of these transporters in cancer, although several mutations have been associated with other diseases. Thus far, reports have linked seven missense mutations in the coding region of EAAT1 to the etiology of extremely rare cases of episodic ataxia type 6 (EA6)[16]. These mutants vary in their degree of loss- or gain-of-function of substrate transport and/or anion conductivity[16]. Moreover, several other EAAT1 mutations and duplications have been associated with other neurological disorders including migraine, ADHD, autism, and Tourette's syndrome[17–19]. To the best of our knowledge, there have been no reports so far that associate mutations of EAAT1 to the development and progression of cancer.

Over the last fifteen years, a growing number of 3D structures have been published for the archaeal glutamate transporter orthologues Glt_{Ph}[20] and Glt_{Tk}[21], as well as human EAAT1[22,23], EAAT2[24] and EAAT3[25], in complex with the endogenous substrate L-aspartate, Na^+ ions and/or inhibitors. Glutamate transporters assemble in obligate homo-trimers of which the protomers operate independently of each other. Each protomer consists of a rigid

trimerization or scaffold domain (scaD) and a dynamic transport domain (tranD) that engages with the substrate and co-transported Na^+ ions[22]. Structures covering inward-facing, intermediate, and outward-facing conformations provide information on the movement of individual transmembrane helices (TMs). Specifically, the flexible helical hairpin 2 (HP2) in tranD controls the access of ligands to the substrate binding site and is an essential 'gate' that upon opening and closing regulates the 'elevator-like' translocation of tranD. Thus, these structures may be used to gain mechanistic insight into the effects of genetic variability on transport function, as was previously demonstrated by mapping genetic variants of glucose (GLUT1) and nucleoside (ENT1) transporters to their respective crystal structures[26].

In this chapter, we characterize a series of EAAT1 somatic mutations that were identified from biopsy material of cancer patients represented in the Genomic Data Commons (GDC) dataset[27]. Using the reported ligand-bound crystal structures of EAAT1[22,23], predictions were made on which variants would most likely impact binding of substrates (L-glutamate and L-aspartate). To determine whether these mutants would affect the binding of potential pharmacological modulators, we included the 'orthosteric' inhibitor TFB-TBOA[28] and the 'allosteric' inhibitor UCPH-101[9], which have both been co-crystalized in EAAT1[22]. The selected eight mutations, together with two EA6-associated mutants (M128R, T318A), were tested *in vitro* for substrate uptake and inhibition using the impedance-based phenotypic assay that was developed in **Chapter 6**. Mutants displayed divergent effects on EAAT1 function, which was apparent from an altered substrate and/or inhibitor potency. Taken together, the results in this work demonstrate 1) the suitability of the label-free phenotypic method to assess functional variation of EAAT1 mutants and 2) the opportunity of using *in silico* techniques to rationalize the *in vitro* phenotype of disease-relevant mutants.

7.2 – Results

7.2.1 – Cancer-related mutations are widespread across the EAAT1 structure

Somatic mutations in EAAT1 are found in cancer patients suffering from different cancer types. Across all cancer types in the Genomic Data Commons (GDC)[27], we identified 105 unique EAAT1 mutations primarily located in uterine cancer (29 mutations) followed by lung cancer and melanoma (21 mutations each) and colon cancer (11 mutations). The frequency of these unique mutations is comparable to natural variance occurrence (1.18% vs. 1.75%, respectively), and they are widespread across the EAAT1 structure without any specific mutational pattern observed per cancer type (**Supplementary Figure 7.S1a,b**). However, most EAAT1 mutations found in cancer patients are not present in natural variance, and some of them are found in structural domains in which conformational rearrangements could lead to transport function impairment. For example, there are mutations located in the vicinity of the binding sites occupied by the substrate and coordinating Na^+ ions, as well as in the HP2 domain (**Supplementary Figure 7.S1a,b**). Moreover, certain mutations found in cancer patients are located in the binding pockets occupied by orthosteric and allosteric EAAT1 inhibitors, which could lead to changes in their binding affinity and potency. We shortlisted 12 mutations not present in natural variance that were found in the

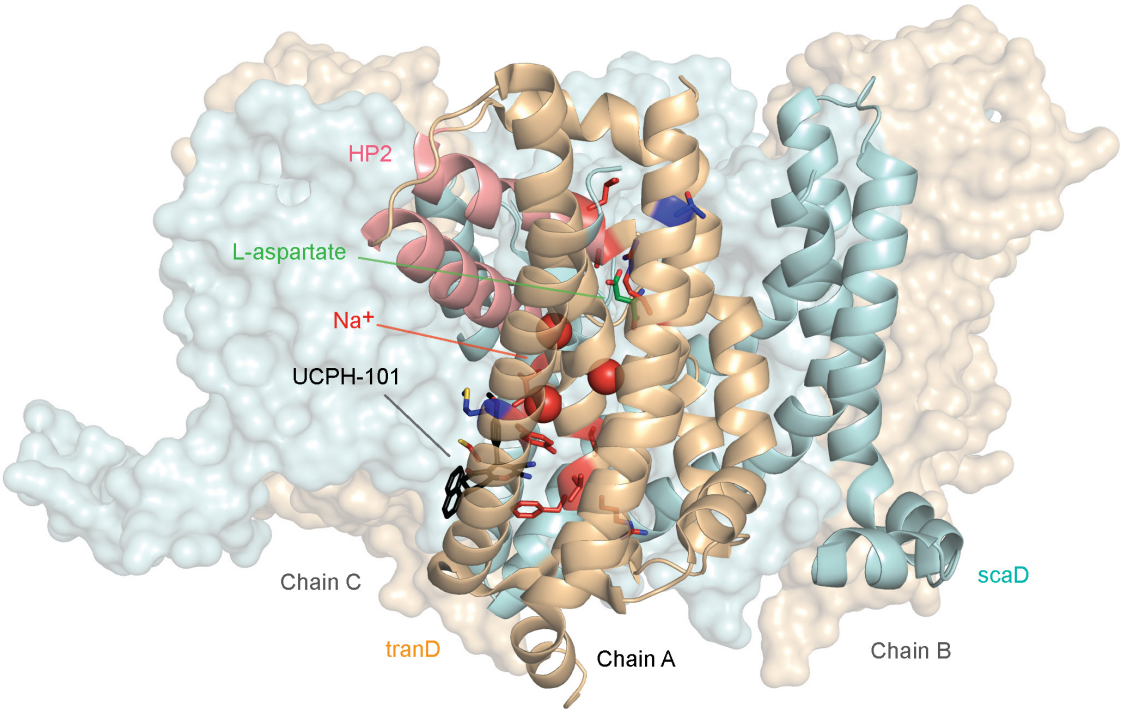

Figure 7.1 – EAAT1 mutations presented in this study. Structural distribution of cancer- and ataxia-related mutants in EAAT1 functionally relevant domains presented in this study. Cancer-related mutations (Y127C, V247F, C252F, R388K, F389L, V390M, P392L, I397V, A446E, A446V, L448Q, and R479W) are mapped in red onto chain A of the EAAT1 trimer (PDB 7AWM). Ataxia-related mutations (M128R and T318A) are mapped in dark blue onto chain A. Chains B and C are represented as surfaces. Protein domains are color-coded as follows: tranD domain (orange), scaD domain (cyan), helical hairpin 2 (HP2) domain (red). The co-crystalized substrate, L-aspartate, is represented in green sticks in chain A. The three coordinated Na^+ ions are represented as red spheres in chain A. The allosteric inhibitor UCPH-101 is represented in black sticks.

functional and binding domains mentioned above (Y127C, V247F, C252F, R388K, F389L, V390M, P392L, I397V, A446E, A446V, L448Q, and R479W) to characterize their effect with a combination of *in silico* and *in vitro* methods (**Figure 7.1**).

7.2.2 – EAAT1 mutants are predicted to have a local effect on substrate and inhibitor binding affinity

The effect on ligand binding affinity of cancer-related mutants found in the orthosteric and allosteric binding sites of EAAT1 was tested *in silico* to prioritize mutations for *in vitro* testing. We calculated changes in binding energy $\Delta\Delta G_{bind}$ for two endogenous substrates (L-aspartate and L-glutamate), one competitive "orthosteric" inhibitor (TFB-TBOA), and one non-competitive "allosteric" inhibitor UCPH-101 (**Table 7.1**). Since the method employed short-range Monte Carlo sampling, we restricted our analysis to mutants in the vicinity of the ligand of interest and classified the mutants as "orthosteric" (V247F, P392L,

Table 7.1 – Binding energy changes ($\Delta\Delta G_{bind}$) predicted in ICM-Pro for EAAT1 orthosteric and allosteric mutants.

	Orthosteric mutants $\Delta\Delta G_{bind}$ (kcal/mol)[a]				Allosteric mutants $\Delta\Delta G_{bind}$ (kcal/mol)[b]
	L-aspartate	L-glutamate	TFB-TBOA		UCPH-101
V247F[c]	0.52	0.08	–0.70	**Y127C**	5.82
P392L	0.04	–0.01	–0.70	**V247F**[c]	0.68
A446E	6.39	–0.90	1.86	**C252F**	–0.49
A446V	0.58	–1.73	2.23	**R388K**	–0.05
L448Q	–0.35	–1.88	1.79	**F389L**	3.83
R479W	7.13	6.42	42.19	**V390M**	–0.76
				I397V	–0.62

[a] ΔΔGbind was calculated for the endogenous substrates L-aspartate and L-glutamate and for the competitive inhibitor TFB-TBOA for orthosteric EAAT1 mutants. The systems used were chain A of PDB 5LLU (with L-aspartate co-crystalized and L-glutamate docked), and chain A of PDB 5MJU (with TFB-TBOA co-crystalized).
[b] For the allosteric mutants, $\Delta\Delta G_{bind}$ was calculated for the allosteric inhibitor UCPH-101 in Chain A of PDB 5MJU.
[c] V247F is situated between the orthosteric and allosteric site

A446E, A446V, L448Q, and R479W, **Figure 7.2a,b**) and "allosteric" (Y127C, V247F, C252F, R388K, F389L, V390M, and I397V, **Figure 7.2c,d**). A positive $\Delta\Delta G_{bind}$ over 1 kcal/mol can be interpreted as a significant decrease in binding affinity, while a negative $\Delta\Delta G_{bind}$ below –1 kcal/mol can be interpreted as a significant increase in binding affinity (**Table 7.1**)[29].

Within the orthosteric mutants, we observed a substantial increase in $\Delta\Delta G_{bind}$ values in mutant R479W for both endogenous substrates and especially for the inhibitor TFB-TBOA, which indicates highly unfavorable binding of these ligands. V247F and P392L did not show significant changes as these residues are further away from the substrate's binding site, but an incipient increased binding affinity towards TFB-TBOA was observed. A446V and L448Q, and to a lesser extent A446E, showed an increased binding affinity towards L-glutamate. Interestingly, while both A446 mutants displayed a reduced TFB-TBOA affinity, A446E and A446V showed a different profile for the two endogenous substrates. A substantial loss of binding affinity towards L-aspartate was observed in A446E, but not A446V. Within the allosteric mutants, Y127C and F389L showed a significant decrease in binding affinity towards UCPH-101. V390M showed the biggest increase in binding affinity, although this change in $\Delta\Delta G_{bind}$ was not significant..

Based on these results, we selected five orthosteric (P392L, A446E, A446V, L448Q, and R479W) and two allosteric mutants (Y127C and V390M) for *in vitro* testing based on their differential $\Delta\Delta G_{bind}$ profiles. Moreover, we included V247F in the selection since it was considered to be at the interface of both binding pockets. Of the selected residues, Y127, V390, P392, A446, L448 and R479 are fully conserved in mammalian EAATs, as well as the archaeal glutamate transporter homolog Glt_{Ph} (except V390 and L448), which suggests the relative importance of these residues in protein function (**Supplementary Figure 7.S2**). To validate the *in vitro* assay, we selected two additional EA6-associated EAAT1 mutations that have been reported to either completely abolish glutamate transport (M128R) or have unaltered transport (T318A). Neither of these two residues are conserved in other

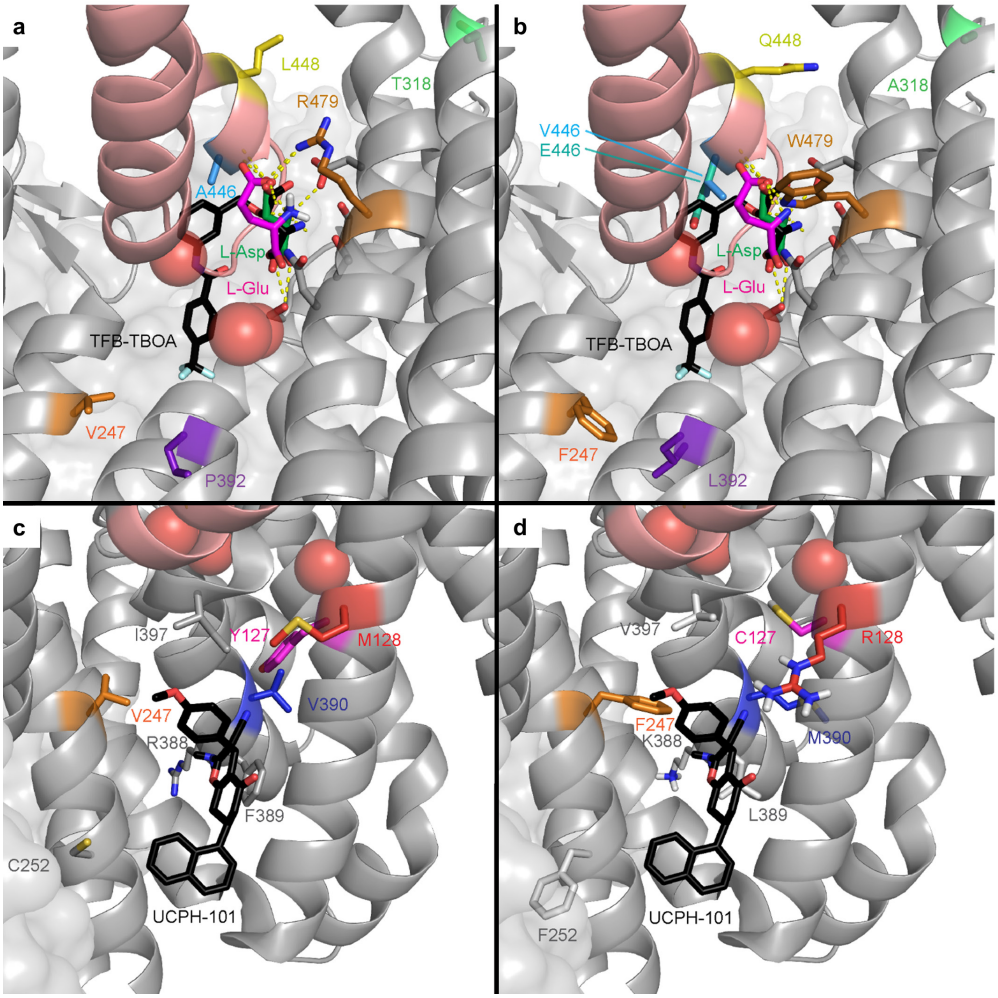

Figure 7.2 – EAAT1 disease-related mutations in the orthosteric and allosteric binding sites. Mutations are mapped onto chain A of PDB 7AWM. Thermostabilizing mutations C252V and T318M were reverted in 7AWM for $\Delta\Delta G_{bind}$ calculation and visualization purposes. For spatial reference, the helical hairpin 2 (HP2) domain helices are colored salmon. The three coordinated Na^+ ions are represented as red spheres. (**a**) Wild-type residues where mutations have been found in cancer in the orthosteric binding site of EAAT1. Ataxia-related reference mutation T318A is visualized in light green. The co-crystalized substrate, L-aspartate, is represented as green sticks. The docked substrate, L-glutamate, is represented in magenta. The competitive inhibitor TFB-TBOA is represented as black sticks and superimposed to the 7AWM structure from its position in PDB 5MJU. Polar contacts between the substrate and EAAT1 are represented as dashed yellow lines. (**b**) Mutated residues in the orthosteric binding site of EAAT1. (**c**) Wild-type residues where mutations have been found in cancer in the allosteric binding site of EAAT1. Ataxia-related reference mutation M128R is visualized in red. The co-crystalized allosteric inhibitor UCPH-101 is represented as black sticks. (**d**) Mutated residues in the allosteric binding site of EAAT1.

glutamate transporters (**Supplementary Figure 7.S2**). M128 is adjacent to Y127 and in close proximity to the binding site of UCPH-101, whereas T318 is not in the vicinity of ligand binding sites (**Figure 7.2**).

7.2.3 – EAAT1 mutants respond differentially to substrates in a phenotypic assay

To assess the selected mutants for their function *in vitro*, we generated a series of HEK293 JumpIn cell lines that were modified to stably express either wild-type ($EAAT1_{WT}$) or mutant EAAT1 upon induction with 1 μg/ml doxycycline for 24 h. None of the ten mutants showed either a decreased or increased expression of the HA-tagged EAAT1 compared to $EAAT1_{WT}$ after doxycycline treatment, indicating that the mutations did not affect translation of the transgene (**Supplementary Figure 7.S3**).

To assess whether the EAAT1 mutants affect transporter functionality, we used the impedance-based phenotypic assay that was developed in **Chapter 6**. In this set-up, adherent cells (over)expressing EAAT1 are cultured on gold-plated electrodes in a 96-well E-plate. Upon stimulation with high concentrations (10 μM – 1 mM) of substrate (i.e., L-glutamate or L-aspartate) the cells started spreading as a result of Na^+-dependent substrate uptake *via* EAAT1 and subsequent cell swelling. The expanded electrode coverage by the cells generated an increase in impedance over time, which was expressed as Cell Index (CI) and interpreted as a readout of EAAT1 function (**Figure 7.3a**). Growth curves were recorded prior to inhibitor pretreatment and substrate stimulation and all mutants displayed similar CI traces compared to $EAAT1_{WT}$, which suggested that the presence of mutant EAAT1 did not substantially affect cell adhesion or proliferation during the experiments (**Supplementary Figure 7.S4**).

L-glutamate induced a concentration-dependent cellular response in $EAAT1_{WT}$ (pEC_{50} = 3.5 ± 0.0), which was reflected by a gradual increase of the normalized Cell Index (nCI) in the first 120 min after substrate stimulation (**Figure 7.3a–d, Table 7.2**). A comparable L-glutamate potency was observed for the EA6 mutant T318A (pEC_{50} = 3.3 ± 0.0) with a slightly increased maximal response (E_{max}), whereas the L-glutamate response was completely abolished for M128R (**Figure 7.3b,d**). The allosteric site mutants V247F (pEC_{50} = 3.8 ± 0.0) and V390M (pEC_{50} = 3.5 ± 0.0) produced similar L-glutamate potencies compared to $EAAT1_{WT}$, where V247F has a 62% reduced E_{max} (**Figure 7.3b**). The potency of L-glutamate on Y127C was enhanced (pEC_{50} = 4.1 ± 0.1), but displayed a substantial drop (94%) in E_{max} (**Figure 7.3b**). The orthosteric site mutants P392L (pEC_{50} = 3.8 ± 0.0) and L448Q (pEC_{50} = 3.3 ± 0.1) showed no significant change in L-glutamate potency, although the concentration-effect curve for L448Q appeared more linear and shifted rightward and did not appear to reach a maximum within the tested concentration range (**Figure 7.3c**). Both A446E and A446V produced glutamate responses with a strongly reduced $E_{max,}$ but with significantly enhanced L-glutamate potency (pEC_{50} = 4.4 ± 0.3 and 4.3 ± 0.2, respectively), whereas no concentration-dependent L-glutamate response was observed for R479W (**Figure 7.3c,d**).

Next, we assessed the responsiveness of the EAAT1 mutants to the endogenous substrate L-aspartate. L-aspartate induced a concentration-dependent cellular response in $EAAT1_{WT}$ (pEC_{50} = 3.6 ± 0.1) similar to L-glutamate (**Figure 7.3e**). The potency of L-aspartate was comparable in the EA6 mutant T318A (pEC_{50} = 3.5 ± 0.0) with an elevated E_{max}, whereas in M128R no L-aspartate response was observed at 1 mM (**Figure 7.3e**). The response of L-aspartate in V390M (pEC_{50} = 3.6 ± 0.0) was identical to $EAAT1_{WT}$ (**Figure 7.3e**).

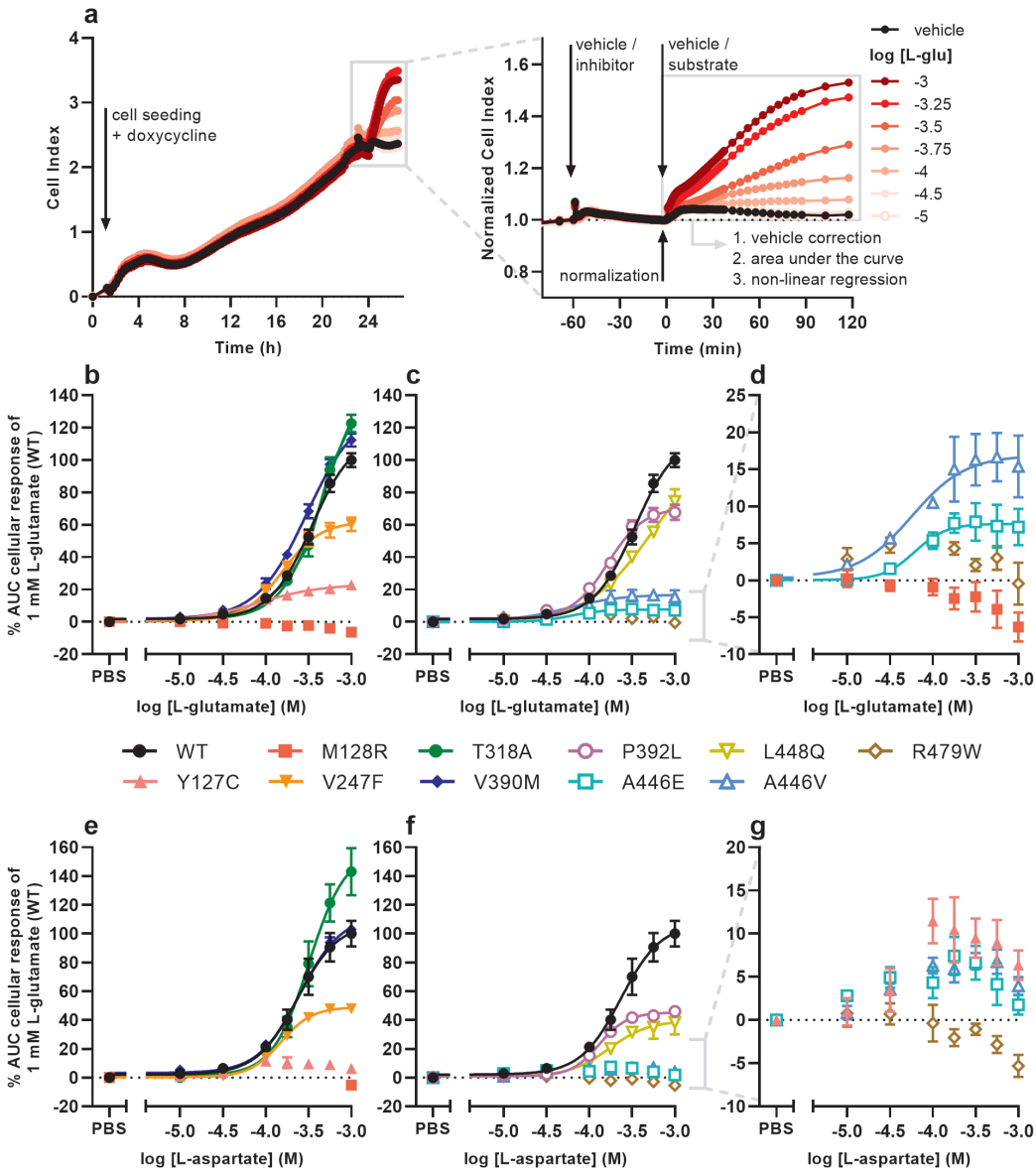

Figure 7.3 – Cellular responses of L-glutamate and L-aspartate in an impedance-based phenotypic assay on $EAAT1_{WT}$ and mutant cells. (**a**) Illustrative graph of the assay and analysis procedure. $EAAT1_{WT}$ cells are seeded and grown for 24 h in the presence of 1 µg/ml doxycycline to induce EAAT1 expression. Cells are pretreated with vehicle (PBS/DMSO) or inhibitor (TFB-TBOA or UCPH-101, only in **Figure 7.4**) for 60 min and subsequently stimulated with vehicle (PBS) or substrate (L-glutamate or L-aspartate) for 120 min. The Cell Index (CI) is normalized prior to substrate stimulation and the cellular response is quantified by analyzing the net area under the curve (AUC). (**b–g**) Concentration-response curves of (**b–d**) L-glutamate and (**e–g**) L-aspartate on $EAAT1_{WT}$ cells and (**b,e**) ataxia and allosteric site mutants and (**c,f**) orthosteric site mutants. (**d,g**) Zoom-in on mutants with low maximal cellular responses. Cellular response is expressed as the net AUC of the first 120 min after L-glutamate or L-aspartate stimulation. Graphs are normalized to the response of 1 mM L-glutamate or L-aspartate on $EAAT1_{WT}$ cells. Data are shown as the mean ± SEM of three to seven individual experiments each performed in duplicate.

Table 7.2 – Potencies (pEC_{50}) of L-glutamate and L-aspartate and inhibitory potencies (pIC_{50}) of TFB-TBOA and UCPH-101 on JumpIn-$EAAT1_{WT}$ and mutant cells in an impedance-based phenotypic assay.

	L-glutamate		L-aspartate		TFB-TBOA	UCPH-101
	pEC_{50}	E_{max} (%) [a]	pEC_{50}	E_{max} (%) [a]	pIC_{50}	pIC_{50}
WT	3.5 ± 0.0	117 ± 5	3.6 ± 0.1	108 ± 9	6.7 ± 0.1	5.4 ± 0.0
Y127C	4.1 ± 0.1 ***	23 ± 3	N.D.	N.D.	6.2 ± 0.0 *	N.D.
M128R	N.D.	N.D.	N.D.	N.D.	N.D.	N.D.
V247F	3.8 ± 0.0	55 ± 9	3.8 ± 0.0	49 ± 1	5.7 ± 0.1 ****	5.3 ± 0.0
T318A	3.3 ± 0.0	156 ± 4	3.5 ± 0.0	158 ± 18	6.9 ± 0.1	5.4 ± 0.0
V390M	3.5 ± 0.0	132 ± 6	3.6 ± 0.0	112 ± 3	6.7 ± 0.0	5.4 ± 0.0
P392L	3.8 ± 0.0	71 ± 4	3.9 ± 0.0	46 ± 3	6.5 ± 0.1	N.D.
A446E	4.4 ± 0.3 ****	8 ± 2	N.D.	N.D.	7.4 ± 0.2 **	5.9 ± 0.2
A446V	4.3 ± 0.2 ****	16 ± 4	N.D.	N.D.	N.D.	N.D.
L448Q	3.3 ± 0.1	116 ± 25	3.7 ± 0.1	47 ± 13	7.9 ± 0.0 ****	5.9 ± 0.1 **
R479W	N.D.	N.D.	N.D.	N.D.	N.D.	N.D.

[a] Maximal responses (E_{max}) are normalized to the cellular response of 1 mM L-glutamate or L-aspartate (100%) on JumpIn-$EAAT1_{WT}$ cells.
Data are presented as the mean ± SEM of three to seven individual experiments each performed in duplicate. Significant differences between potencies of WT and mutant cells were determined using a one-way ANOVA with Dunnett's post-hoc test. * $p < 0.05$, ** $p < 0.01$, *** $p < 0.001$, **** $p < 0.0001$, N.D. = not determined.

The mutants V247F (pEC_{50} = 3.8 ± 0.0), P392L (pEC_{50} = 3.9 ± 0.0) and L448Q (pEC_{50} = 3.7 ± 0.1) produced similar L-aspartate potencies, but a substantially lowered E_{max} (~60%) compared to $EAAT1_{WT}$ (**Figure 7.3e,f**). For Y127C, A446E and A446V a much reduced L-aspartate response was observed which dropped at high concentrations, resulting in a bell-shaped concentration-effect curve (**Figure 7.3e–g**). Similar to L-glutamate, no L-aspartate response was observed for R479W (**Figure 7.3f,g**). Collectively, these data demonstrate that the selected EAAT1 mutants impact L-glutamate and L-aspartate transport.

7.2.3 – EAAT1 mutants respond differentially to substrates in a phenotypic assay

To assess whether the selected mutants modulated the effects of the competitive ('orthosteric') inhibitor TFB-TBOA and the non-competitive ('allosteric') inhibitor UCPH-101, we pretreated the cells for 1 h with increasing concentrations of inhibitor prior to stimulation with 1 mM L-glutamate. In $EAAT1_{WT}$, inhibitor pretreatment itself did not result in substantial changes in the nCI (**Supplementary Figure 7.S5c–f**). Strikingly, the M128R pretreatment with TFB-TBOA resulted in a concentration-dependent sharp nCI increase which peaked after 10–30 min, whereas pretreatment with UCPH-101 induced a more gradual nCI increase that plateaued after 60 min (**Supplementary Figure 7.S5a,b**). These inhibitor responses were not observed in any of the other mutants, although V247F, A446E and A446V showed concentration-dependent decreases of the nCI upon TFB-TBOA pretreatment, which were substantially lower in magnitude compared to M128R (**Supplementary Figure 7.S5d,f**). This suggests that M128R displays a distinct physiological phenotype compared to $EAAT1_{WT}$ and other mutants.

To elucidate a potential mechanism behind the M128R response to both inhibitors, we assessed whether the inhibitors displayed any interaction with each other or the substrate L-glutamate. Indeed, cells pretreated with TFB-TBOA were responsive to a subsequent stimulation with UCPH-101 and *vice versa*, indicating that the cellular responses elicited by either inhibitor are additive and are constituted by independent mechanisms (**Supplementary Figure 7.S6a,b**). Interestingly, the response caused by TFB-TBOA pretreatment was completely blocked after stimulation with 1 mM L-glutamate and a TFB-TBOA response was prevented when cells were pretreated with L-glutamate, indicating that the TFB-TBOA response is transient and originates from interactions at the substrate binding site (**Supplementary Figure 7.S6a,c**). In contrast, L-glutamate stimulation after UCPH-101 pretreatment does not reduce the nCI. The UCPH-101 response after L-glutamate pretreatment has a comparable magnitude to the UCPH-101 pretreatment on its own, suggesting that L-glutamate and UCPH-101 do not compete for the same binding site (**Supplementary Figure 7.6b,c**). In addition, the Na^+/K^+-ATPase (NKA) inhibitor ouabain prevented any inhibitor- or substrate-induced cellular responses in M128R cells, which indicates that TFB-TBOA and UCPH-101 responses are likely dependent on ion influx (**Supplementary Figure 7.6d**).

7.2.5 – EAAT1 mutants alter TFB-TBOA and UCPH-101 inhibition

For $EAAT1_{WT}$ and all other mutants, except M128R, we assessed the inhibitory potencies of TFB-TBOA and UCPH-101 by analyzing the response of 1 mM L-glutamate after 60 min pretreatment with increasing inhibitor concentrations. In $EAAT1_{WT}$, TFB-TBOA inhibited the L-glutamate response in a concentration-dependent manner (pIC_{50} = 6.7 ± 0.1) (**Figure 7.4a,b, Table 7.2**). The EA6 mutant T318A (pIC_{50} = 6.9 ± 0.1), allosteric site mutant V390M (pIC_{50} = 6.7 ± 0.0) and orthosteric site mutant P392L (pIC_{50} = 6.5 ± 0.1) did not affect the inhibitory potency of TFB-TBOA (**Figure 7.4a,b**). Both Y127C (pIC_{50} = 6.2 ± 0.0) and V247F (pIC_{50} = 5.7 ± 0.1) significantly decreased the potency, whereas L448Q (pIC_{50} = 7.9 ± 0.0) significantly enhanced the inhibitory potency of TFB-TBOA (**Figure 7.4a,b**). Interestingly, A446E was susceptible to TFB-TBOA inhibition, showing an increased inhibitory potency (pIC_{50} = 7.4 ± 0.2), whereas A446V as well as R479W did not display any sigmoidal concentration-dependent inhibition by TFB-TBOA (**Figure 7.4b,c**).

The effects of EAAT1 mutants on UCPH-101 inhibition were different from TFB-TBOA. In $EAAT1_{WT}$, UCPH-101 could inhibit the response of L-glutamate in a concentration-dependent manner (pIC_{50} = 5.4 ± 0.0) (**Figure 7.4d,e, Table 7.2**). V247F (pIC_{50} = 5.3 ± 0.0), T318A (pIC_{50} = 5.4 ± 0.0) and V390M (pIC_{50} = 5.4 ± 0.0) did not affect L-glutamate response inhibition by UCPH-101 (**Figure 7.4d**). In Y127C, P932L, A446V and R479W UCPH-101 was unable to inhibit the L-glutamate response at any of the tested concentrations, indicating a loss of the UCPH-101 interaction (**Figure 7.4d–f**). Similar to TFB-TBOA, both L448Q (pIC_{50} = 5.9 ± 0.1) and A446E (pIC_{50} = 5.9 ± 0.2) enhanced the inhibitory potency of UCPH-101, although this was not significant for A446E (p = 0.0919) (**Figure 7.4e,f**). Taken together, these data imply that the selected EAAT1 mutants differentially modulate both substrate and EAAT1 inhibitor interactions.

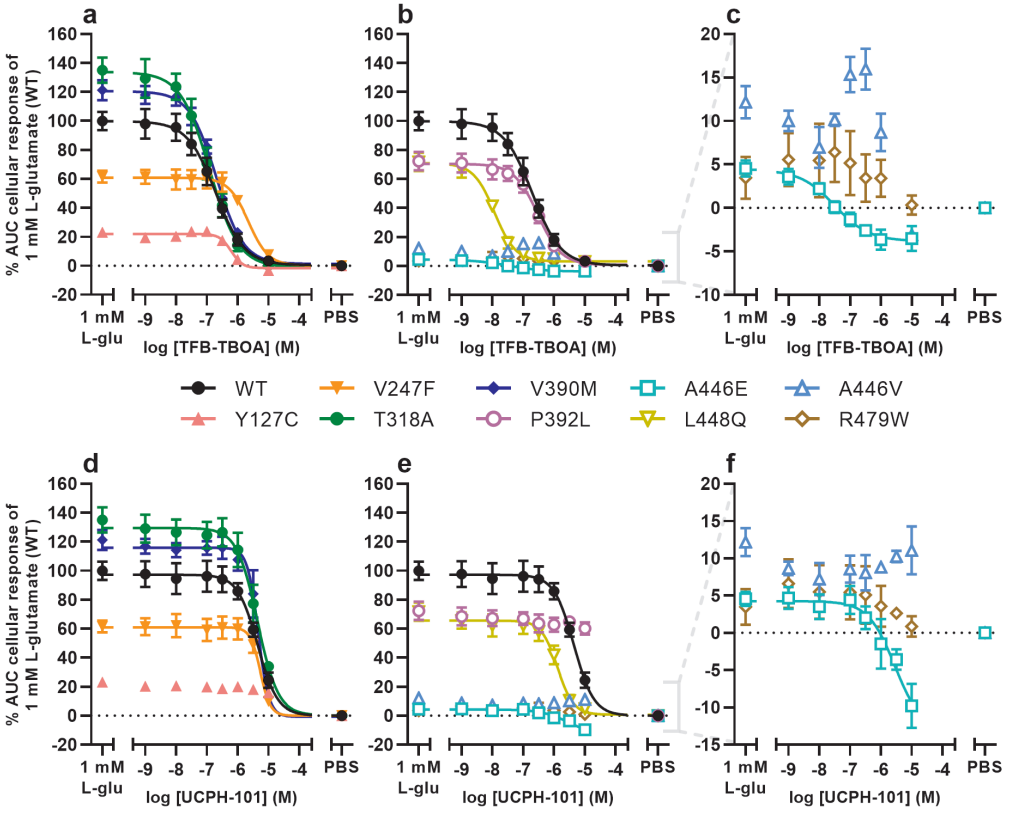

Figure 7.4 – Inhibition of L-glutamate responses by TFB-TBOA and UCPH-101 in an impedance-based phenotypic assay on $EAAT1_{WT}$ and mutant cells. (**a–f**) Concentration-inhibition curves of (**a–c**) TFB-TBOA and (**d–f**) UCPH-101 on $EAAT1_{WT}$ cells and (**a,d**) ataxia and allosteric site mutants, and (**b,e**) orthosteric site mutants. (**c,f**) Zoom-in on mutants with low maximal cellular responses. Cells were pretreated with TFB-TBOA, UCPH-101 or vehicle (PBS/DMSO) for 60 min and stimulated with a submaximal concentration (EC_{80}) of 1 mM L-glutamate or vehicle (PBS) for 120 min. Cellular response is expressed as the net AUC of the first 120 min after L-glutamate stimulation and graphs are normalized to the response of 1 mM L-glutamate on $EAAT1_{WT}$ cells. Data are shown as the mean ± SEM of three individual experiments each performed in duplicate.

7.3 – Discussion

The role of glutamate and aspartate in cancer is increasingly appreciated[30]. Indeed, the regulation of intra- and extracellular levels of these amino acids by EAATs and other transporters, in respect to the tumor microenvironment, is the subject of ongoing investigations. So far, altered function of EAAT1 as a result of single missense mutations has been linked to several extremely rare cases of episodic ataxia type 6 (EA6)[16]. However, there have been no reports on the contribution of genetic variants of EAATs to the development of cancer, and it remains a question to what degree loss- or gain-of-function mutations in these transporters are relevant for disease progression. In this study we identified 105 unique somatic mutations in cancer patients, none of which occurred as natural variants. Although we could not associate the genotype to disease etiology, we observed distinctive cellular responses of eight cancer-associated and two reference EA6-related EAAT1 missense mutants in a label-free phenotypic assay, which together with structural insights provides an initial understanding of altered transporter function and cell behavior.

All EAAT1 mutants were expressed at similar relative levels compared to $EAAT1_{WT}$, which suggests that the introduced mutations did not affect the translation of the protein (**Supplementary Figure 7.S3**). Interestingly, in previous studies several EAAT1 mutants displayed attenuated or increased glutamate uptake activity as a result of reduced (P290R, M128R[16,31]) or enhanced (E219D, T318A[16,17]) surface membrane density, respectively. Indeed, in our functional assay T318A showed a considerable increase in substrate E_{max} (**Figure 7.3b,e, Table 7.2**), which may be attributed to an enhanced membrane insertion of EAAT1[16]. Most other mutants displayed a substantial decrease in substrate E_{max}, with the maximal response being generally lower for L-aspartate than L-glutamate. To address the contribution of amino acid substitutions to their predicted effect on ligand binding affinity (**Table 7.1**) and the observed changes in substrate and/or inhibitor potency (**Figure 7.3–7.4, Table 7.2**), we will discuss each mutant individually.

Tyr at position 127 is located in TM3 and is conserved in all human EAATs and the archaeal Glt_{Ph} (**Supplementary Figure 7.S2**), where the backbone carboxylate of Tyr is part of the third Na^+ binding site (Na3)[23,25,32]. Substitution of Y127 to Cys does not affect the ability of EAAT1 to translocate substrate, as we observed a concentration-dependent cellular response of L-glutamate in Y127C cells, albeit with a substantially reduced E_{max} (**Figure 7.3b**). In addition to forming Na3, Y127 forms a hydrogen bond with the carbonitrile group of UCPH-101[22]. This bond likely cannot form in Y127C, which results in a loss of UCPH-101 inhibition (**Figure 7.4d**). In line with this, mutation of Y127 to Phe, Leu, Ile or Arg showed a significant drop in pIC_{50} of UCPH-101 in a [^{3}H]-D-aspartate uptake assay[33]. The slight reduction of TFB-TBOA potency suggests that Y127C stabilizes a transporter conformation that affects the binding of the bulky inhibitor, but not the substrate.

M128 is adjacent to Y127 and is exposed to membrane lipids. The M128R mutation was found in an EA6 patient and patch clamp experiments demonstrated that M128R shows a complete loss of glutamate uptake as well as abolished anion currents that could not be explained by slightly reduced surface expression levels[16]. Indeed, we did not detect any

L-glutamate or L-aspartate responses in M128R (**Figure 7.3b,e**), which suggests that this mutant is likely transport incompetent. Surprisingly, we observed substantial concentration-dependent positive cellular responses when M128R cells were treated with TFB-TBOA or UCPH-101, which were not observed in $EAAT1_{WT}$ or other mutants (**Supplementary Figure 7.S5**). A recent study demonstrated that mutation of M128 to Arg may inflict two potential disruptions to EAAT1[34]. The positively charged Arg could flip towards the 'inside' of the protein and disrupt the binding of Na^+ to Na3. Occupation of this site by Na^+ is crucial to initiate substrate binding and translocation[35], which may explain the absence of glutamate transport in M128R. Secondly, the Arg in M128R could flip 'outward' towards the lipid bilayer. Molecular dynamics (MD) simulations revealed a local membrane deformation resulting from attraction of polar lipid head groups to the Arg, which recruited a density of water molecules halfway into the bilayer[34]. This may provide a pathway for Na^+ ions that enter the Na3 site to leak into the cytosol, which could result in cell volume increase and subsequent morphological changes, as we have shown in **Chapter 6**. Thus, we hypothesize that binding of TFB-TBOA or UCPH-101 to EAAT1 M128R stabilizes an Arg 'outward' conformation that allows uncoupled Na^+ influx, which results in a phenotypic response in the absence of substrate (**Supplementary Figure 7.S5–7.S6**). To our knowledge, this is the first report of inhibitor-induced functional responses in glutamate transporters, which warrants further investigation and could hold promise for future therapeutic strategies.

The Val at position 247 is located in TM4c at the scaD–tranD interface, which contains mostly hydrophobic residues conferring the selectivity of UCPH-101 towards EAAT1[22]. Mutation to Phe did not alter L-glutamate and L-aspartate responses (**Figure 7.3**), which indicates that V247F conserves substrate translocation. Moreover, UCPH-101 inhibition was unaffected in V247F (**Figure 7.4d**) which suggests that V247 is not crucial to inhibitor binding at the allosteric site. Interestingly, the inhibitory potency of TFB-TBOA was significantly reduced in V247F (**Table 7.2**), contrary to *in silico* predictions showing a slightly enhanced TFB-TBOA binding affinity, if at all (**Table 7.1**). Increasing the bulkiness of the residue may indirectly compromise the size of the hydrophobic cavity that accommodates the trifluoromethyl moiety of TFB-TBOA. This would result in a less favorable orientation of the inhibitor and a reduced affinity for the substrate binding site.

T318A was identified in a patient with episodic ataxia, although there is no evidence that this mutation is pathogenic[34,36]. Located in TM6 of the tranD, the Thr in $EAAT1_{WT}$ is not involved with substrate or Na^+ binding sites or subdomain movements. Mutation to Ala increased glutamate uptake and anion currents as a result of increased surface expression of the transporter[16,34]. Besides an increased substrate E_{max}, we did not observe any significant changes in substrate and inhibitor potency, which suggests that T318A does not alter the function of EAAT1.

V390 is located in TM7a of tranD and is adjacent to F389 and V393, which both make hydrophobic interactions with the chromene scaffold of UCPH-101[22]. Substrate responses and inhibition by UCPH-101 and TFB-TBOA in V390M were nearly identical to $EAAT1_{WT}$, which indicates that the introduction of a Met in this position is conservative and does not alter transport function.

The Pro at position 392 is located in TM7a near V390 and is completely conserved throughout the SLC1 family and Glt_{Ph}[22]. P392 is part of the scaD–tranD interface that lines the hydrophobic cavity of the chloride conductive pathway[37,38]. Mutation of P392 to small hydrophobic residues (Ala, Val) resulted in slightly increased substrate affinities and anion conductances[39], which may be reflected by a small increase in pEC_{50} for L-glutamate and L-aspartate in P392L (**Table 7.2**). Strikingly, while TFB-TBOA binding is unaffected, P392L causes a complete loss of UCPH-101's inhibition of the L-glutamate response (**Figure 7.4b,e, Table 7.2**). P392 neighbors F389 and V393, which create hydrophobic interactions with the chromene skeleton of UCPH-101[22]. Mutation to a slightly bulkier Leu might correct the disruption in the helical turn caused by Pro in TM7a and promote an increase in helix rigidity that displaces the location of the nonpolar residues in this region, which substantially reduces the affinity of UCPH-101 for this site.

Three mutations (A446E, A446V and L448Q) are located in HP2, which is an important structural element that regulates the access of Na^+ and substrate to their binding sites[20,22]. In the HP2-closed conformation, the backbone amine of A446 hydrogen bonds with the sidechain carboxylate of L-aspartate [22]. In our phenotypic assay both A446E and A446V displayed vastly reduced maximal substrate responses but significantly increased affinities (**Table 7.2**), which could be the result of low surface expression or a reduced turnover rate[40]. Notably, mutation to Val at this position abrogates L-glutamate response inhibition, whereas a Glu substitution results in a significantly enhanced potency of TFB-TBOA (**Figure 7.4c,f, Table 7.2**). We hypothesize that a bulkier Val sterically clashes with the benzoxyl moiety of TFB-TBOA, which destabilizes the interaction of the inhibitor with HP2 that results in a more flexible 'open' conformation of HP2 and reduced binding affinity of the inhibitor[22]. Contrarily, a negatively charged Glu might engage in electrostatic interactions with the amide of the benzoylamine moiety of TFB-TBOA, which could stabilize a more favorable 'open' HP2 conformation.

The adjacent HP2 residue L448 is involved in HP2 backbone flexibility, which is essential for K^+-dependent re-translocation of the tranD during the transport cycle[41]. Strikingly, the pIC_{50} for both TFB-TBOA and UCPH-101 are markedly increased in L448Q. In a previous study, mutation of L448 to Cys reduced L-glutamate affinity and maximal transport rate, but it significantly enhanced the inhibitory potency of the competitive inhibitor DL-TBOA[42]. Similar to A446E, it is likely that the introduction of a polar residue in HP2 may stabilize an 'open' TFB-TBOA-bound conformation, but to a lesser extent a 'closed' substrate-bound conformation. Moreover, the enhanced pIC_{50} for both UCPH-101 and TFB-TBOA may be the result of a reduced affinity of L-glutamate in the orthosteric site, which could augment the apparent inhibitory potency.

The Arg at position 479 confers substrate selectivity and is conserved among glutamate/aspartate transporters. The guanidinium group of R479 forms a hydrogen bond with the sidechain carboxylate of the substrate during translocation[22]. Moreover, R479 forms a salt bridge with E406 in TM7 during K^+ re-translocation, which sterically hinders closure of HP2 and substrate binding[23,41]. Neutralization of R479 (i.e., mutation to Ala) renders EAAT1 K^+-independent and results in drastically reduced glutamate/aspartate affinity[41],

which was also observed in Glt_{Ph} upon mutation of Arg to Cys[43]. Although R479W may still be able to form a hydrogen bond with the substrate carboxylate, the bulkiness of the indole moiety likely disrupts the electrostatic interactions in the binding site, which leads to a loss of substrate activity (**Figure 7.2b**). This was evident from the relatively high $\Delta\Delta G_{bind}$ values for R479W compared to other mutated residues (**Table 7.1**), which indicate a substantially reduced ligand binding affinity.

Taken together, we provide functional assessments of eight EAAT1 mutations that were found in cancer patients, as well as two EA6-associated mutations. We observed divergent effects of EAAT1 variants on substrate-induced cellular responses, as well as orthosteric and allosteric inhibition, in an impedance-based phenotypic assay. These results warrant follow-up experiments that investigate alterations in anion conductivity and substrate transport kinetics, which could help to explain our functional observations. Moreover, while mutations in a ligand binding site may disrupt or stabilize ligand interactions, they could potentially lead to 'allosteric' effects *via* disruption of conserved interaction networks[44]. Although we have provided hypotheses on the effects of genetic variants based on literature and available 3D structures, we currently lack information on transporter dynamics to substantiate allosteric effects of these EAAT1 mutants. Ongoing MD simulations on substrate-, Na^+- and inhibitor-bound EAAT1 structures may provide insight into the effects of mutated residues on subdomain dynamics. Importantly, in order to allocate these missense variants to a substantial involvement in cancer development and progression we require translational studies that link genotype to phenotype. Thus, the methods presented in this chapter may aid in the identification of pathogenic transporter variants, which may have implications for the development of selective and efficacious therapeutics.

7.4 – Materials & methods

7.4.1 – Materials

Modified Jump In T-REx HEK 293 (JumpIn) cells overexpressing human wild-type ($EAAT1_{WT}$) or mutant EAAT1 (see **section 7.4.6–7.4.9**) were kindly provided by the RESOLUTE consortium (Research Center for Molecular Medicine, Medical University of Vienna, Austria). L-glutamic acid monosodium salt monohydrate, L-aspartic acid monosodium salt monohydrate, doxycycline hyclate, Dulbecco's modified Eagle's medium (DMEM) and Dulbecco's phosphate-buffered saline (PBS) were purchased from Sigma Aldrich (St. Louis, MO, USA). 2-amino-4-(4-methoxyphenyl)-7-(naphthalen-1-yl)-5-oxo-5,6,7,8-tetrahydro-4H-chromene-3-carbonitrile (UCPH-101) was purchased from Santa Cruz Biotechnology (Dallas, TX, USA). (2S,3S)-3-[3-[4-(trifluoromethyl)benzoylamino] benzyloxy] aspartate (TFB-TBOA) was purchased from Axon Medchem (Groningen, The Netherlands). Lipofectamine 3000, P3000 buffer, Gateway LR Clonase II enzyme mix and Proteinase K solution were purchased from ThermoFischer (Waltham, MA, USA). QuikChange II kit was purchased from Agilent Technologies (Santa Clara, CA, USA). QIAprep Spin Miniprep Kit was purchased from QIAGEN (Hilden, Germany). xCELLigence PET E-plates 96 (Agilent Technologies, Santa Clara, CA, USA) were

purchased from Bioké (Leiden, The Netherlands). All other chemicals were of analytical grade and obtained from standard commercial sources.

7.4.2 – Selection of cancer-related mutations

Cancer-related mutations were obtained from the Genomic Data Commons[27] version 22.0 released on January 16th 2020, as re-compiled by Bongers *et al.*[45] Somatic missense mutations were retrieved for gene SLC1A3 (EAAT1) in all cancer types. The 105 unique mutations found were mapped onto the 3D structure of EAAT1 (PDB 5LLU, 5MJU[22] and 7AWM[23]), with particular attention to the functional motifs and binding sites defined by Canul-Tec *et al.*[22,23] Two sets of mutations of interest were defined by visual inspection in the proximity (i.e., 5 Å from co-crystalized ligands) of the orthosteric binding site – occupied by the substrate L-aspartate – and allosteric binding site – occupied by allosteric inhibitor UCPH-101. The "orthosteric" set of mutations included P392L, A446E, A446V, L448Q, and R479W. The "allosteric" set of mutations included Y127C, C252F, R388K, F389L, V390M, and I397V. Additionally, mutation V247F is located at the interface of the two sites and was therefore included in both sets.

As reference, we retrieved SLC1A3 (EAAT1) mutations found in natural variance in the 1000 Genomes dataset[46]. This dataset was obtained from the Uniprot variance database in October 2020[47]. For the purpose of comparison, we calculated the percentage of mutations in EAAT1 found in cancer patients and natural variance by dividing the number of mutations in EAAT1 by the number of patients in each dataset (10,179 and 3,202, respectively) and multiplying it by 100%.

7.4.3 – System preparation and molecular docking

The monomeric EAAT1 systems for binding affinity change predictions were prepared from chain A in PDB codes 5LLU and 5MJU[22] in ICM-Pro version 3.9-2c (Molsoft LLC, San Diego)[48,49]. The systems were prepared by optimizing the protonation states and orientation of histidine and cysteine residues, and the orientation of glutamine and asparagine residues. Moreover, the position of hydrogen atoms was sampled and optimized. Stabilizing mutations in residues selected for further analysis were reverted (i.e., C252V, T318M). We subsequently prepared L-glutamate by adding hydrogen atoms and assigning atomic charges and docked it into the orthosteric binding site of PDB 5LLU, originally occupied by L-aspartate. Upon removal of L-aspartate from the binding site, docking was performed with default settings and 10 poses stored by defining the residues surrounding L-aspartate as the binding site. We analyzed the poses in light of the experimental data available, docking scores, and interaction patterns. The pose with the highest docking score was selected for further analysis.

7.4.4 – Binding affinity change predictions

To prioritize mutations for in vitro testing, we predicted changes in EAAT1 binding affinity to endogenous substrates L-aspartate and L-glutamate, and the inhibitors TFB-TBOA (competitive) and UCPH-101 (allosteric) caused by point mutations. We performed this

analysis in ICM-Pro as follows. The difference in binding energy ($\Delta\Delta G_{bind}$, in kcal/mol) is calculated as the difference between the Gibbs binding energy (ΔG_{bind}, in kcal/mol) in the mutant and the wild-type. ΔG_{bind} is calculated for fixed backbone and Monte Carlo-sampled flexible side chains in the vicinity of the mutated residue as the energy of the protein-ligand complex minus the energy of the protein and ligand separately.

For the cancer-related mutations found in the orthosteric binding site (P392L, A446E, A446V, L448Q, and R479W), we calculated $\Delta\Delta G_{bind}$ for endogenous ligands L-aspartate and L-glutamate (previously docked) in system 5LLU. Moreover, we calculated $\Delta\Delta G_{bind}$ for the competitive inhibitor TFB-TBOA in system 5MJU. For the cancer-related mutations found in the allosteric binding site (Y127C, C252F, R388K, F389L, V390M, and I397V), $\Delta\Delta G_{bind}$ was calculated for the allosteric inhibitor UCPH-101 in system 5MJU. For V247F, which is at the interface of both ligand binding sites, $\Delta\Delta G_{bind}$ was calculated for L-glutamate, L-aspartate, TFB-TBOA and UCPH-101 as described above.

7.4.5 – Structural visualization

All visualizations of EAAT1 structures were generated in PyMOL version 1.3 (Schrödinger LTD) using PDB 7AWM. Where TFB-TBOA was visualized, PDB 5MJU was superimposed on 7AWM.

7.4.6 – Mutagenesis

DNA primers for EAAT1 mutants were designed with a single or double base pair substitution for the resultant amino acid using the QuikChange Primer Design Program and synthesized by Integrated DNA Technologies (IDT, Leuven, Belgium) (**Table 7.3**). Site-directed mutagenesis was performed using a QuikChange II kit. In brief, per mutant 50 ng template DNA (codon-optimized ORF for EAAT1 (SLC1A3) in a pDONR221 vector (pDONR221-SLC1A3, Addgene #131889)) together with 10 μM forward and reverse primer, 1 μl dNTP mix, 2.5 μl 10x reaction buffer and 2.5 U DNA polymerase were run in a PCR thermal cycler for 22 cycles (each cycle consisted of 30 s 95°C, 1 min 55°C, 10 min 68°C). Non-mutated DNA was removed by addition of 5 U DpnI restriction enzyme for 2 h at 37°C. Mutant DNA was transformed into XL1-Blue competent cells in the presence of 50 μg/ml kanamycin for selection. Plasmid was isolated using a QIAprep Spin Miniprep Kit verified by Sanger sequencing (Leiden Genome Technology Center, Leiden, The Netherlands).

7.4.7 – Gateway cloning

To allow stable transfection into JumpIn cells, the wild-type (WT) and mutant pDONR221-SLC1A3 plasmids were cloned into a pJTI R4 DEST CMV TO pA expression vector with a C-terminal Twin-Strep-tag and a hemagglutinin (HA)-tag using Gateway cloning. The expression vector contains a tet-operon (TO) that allows doxycycline (dox)-inducible expression of the transgene. In brief, 150 ng pDONR221-SLC1A3 plasmid and 150 ng pJTI R4 DEST CMV TO pA in TE buffer (10 mM Tris, 1 mM EDTA) were incubated with Gateway LR Clonase II enzyme mix at 25°C for 1 h. To remove endogenous nucleases,

Table 7.3 – DNA primers (forward and reverse) that were used to generate eight cancer-related and two ataxia-related EAAT1 mutants. Mutated bases are bolded.

Mutant	Forward primer (5')	Reverse primer (5')
Y127C	GAGAGCCGTGGTGTACT**G**TATGACCACAACCATCA	TGATGGTTGTGGTCATA**C**AGTACACCACGGCTCTC
M128R	TGAGAGCCGTGGTGTACTATA**G**GACCACAACCAT	ATGGTTGTGGTC**C**TATAGTACACCACGGCTCTCA
V247F	AATGCCCTGGGCCTG**TT**C**C**GTGTTCAGCATGTGC	GCACATGCTGAACAC**G**AA**A**CAGGCCCAGGGCATT
T318A	CAGCTGGCCATGTAC**G**CCGTGACAGTGATCG	CGATCACTGTCACGG**C**GTACATGGCCAGCTG
V390M	GACAAGCGGGTGACCAGATTT**A**TGCTGCCAGTG	CACTGGCAGCA**T**AAATCTGGTCACCCGCTTGTC
P392L	CAGATTTGTGCTGC**T**AGTGGGCGCCACCA	TGGTGGCGCCCACT**A**GCAGCACAAATCTG
A446E	CAGGCATCCCACAGG**AA**GGCCTGGTGACCATG	CATGGTCACCAGGCC**TT**CCTGTGGGATGCCTG
A446V	GCATCCCACAGG**T**CGGCCTGGTGAC	GTCACCAGGCCG**A**CCTGTGGGATGC
L448Q	CACAGGCCGGCC**A**GGTGACCATGGT	ACCATGGTCACC**T**GGCCGGCCTGTG
R479W	GGTTTCTGGATAGGCTG**T**G**G**ACAACCACAAACGTGCT	AGCACGTTTGTGGTTGT**C**C**A**CAGCCTATCCAGAAACC

the mixture was incubated with a Proteinase K solution for 10 min at 37°C. The resulting vectors (WT or mutant pJTI-SLC1A3) were transformed into XL1-Blue competent cells in the presence of 100 μg/ml ampicillin for selection. Plasmid was isolated and sequenced as described in the previous section.

7.4.8 – Cell culture

JumpIn-EAAT1 cells were split twice per week to 10 cm dishes in culture medium (high glucose DMEM containing 10% fetal calf serum, 2 mM Glutamax, 100 IU/ml penicillin and 100 μg/ml streptomycin) at 37°C and 5% CO_2. After thawing and recovery, cells were grown for 3–5 days in culture medium with 5 μg/ml blasticidin and 2 mg/ml G418 before switching to culture medium.

7.4.9 – Generation of stably transfected WT and mutant JumpIn-EAAT1 cells

JumpIn cells were seeded at 90,000 cells/well in culture medium onto a 24-well culture plate and grown within 24 h to 60–70% confluence. Per mutant or WT, a mix of 1.8 μl P3000 buffer, 450 μg pJTI R4 Integrase plasmid and 450 μg pJTI-SLC1A3 plasmid in Opti-MEM was added to a mix of 2.1 μl Lipofectamine 3000 in Opti-MEM (90 μl total per condition) and incubated for 5 min at RT. As a control for antibiotic selection, one dish of cells was incubated with sterile water instead of pJTI-SLC1A3. Cells were transfected with 60 μl of the total mix. On the next day the transfection medium was replaced by fresh culture medium. After 24 h cells were trypsinized and seeded onto 6 cm culture dishes at 200,000 cells/well to grow for 3–4 days. When 70% confluence was reached medium was replaced with selection medium (culture medium with 1 mg/ml G418) to select for successfully transfected cells. Selection medium was refreshed every 2–3 days for 2 weeks until non-transfected cells were all dead and colonies had grown in the transfected dishes. Colonies were resuspended in selection medium and grown to confluence before cryofreezing pools of transfected cells. Prior to use in experiments, cells were cultured in regular culture medium for at least 24 h.

7.4.10 – Whole-cell HA-tag ELISA

To determine the relative amount of C-terminal HA-tagged protein expressed in doxycycline (dox)-induced JumpIn-EAAT1 WT and mutant cells, an enzyme-linked immunosorbent assay (ELISA) was performed on whole, permeabilized cells. Each condition was tested in quintuplicate per experiment. Cells were seeded in culture medium onto a 96-well culture plate coated with 0.1 mg/ml poly-D-lysine at 60,000 cells/well in the presence or absence of 1 μg/ml dox (100 μl total volume) and were grown for 22–24 h at 37°C and 5% CO_2. Cells were washed with PBS and fixed with 4% formaldehyde for 10 min, then washed with Tris-buffered saline (TBS). To allow access of the antibodies to the intracellular HA-tag, cells were incubated with permeabilization buffer (TBS + 0.5% Tween-20 (TBST), 2% bovine serum albumin (BSA) and 0.2% saponin) for 60 min at RT. After blocking and permeabilization, cells were incubated with 1:2500 rabbit anti-HA polyclonal antibody (Invitrogen, Carlsbad, CA, USA) for 60 min at RT and washed with TBST. Subsequently, cells were incubated for with 1:3000 goat anti-rabbit horse radish peroxidase (HRP)-conjugated IgG antibody (Brunschwig Chemie, Amsterdam, The Netherlands) for 30 min at RT and washed with TBS. Immunoreactivity was visualized by addition of 3,3',5,5'-tetramethylbenzidine (TMB) for 2.5 min at RT and subsequent quenching with 1 M H_3PO_4. Absorbance was measured at 450 nm using a Wallac EnVision multimode plate reader (PerkinElmer, Groningen, The Netherlands).

7.4.11 – Impedance-based phenotypic assay

To measure functional substrate responses and substrate inhibition on WT and mutant JumpIn-EAAT1 cells, we employed the label-free impedance-based phenotypic assay as described previously in **Chapter 6**. We used an xCELLigence real-time cell analyzer (RTCA) system (Agilent Technologies, Santa Clara, CA, USA) to record real-time changes in cell morphology. The assay principle is that EAAT1-mediated, Na^+-dependent substrate influx induces cell swelling, which leads to cell spreading. This results in an increased cellular impedance over time and as such is a readout of transporter function. For the assay, JumpIn-EAAT1 cells are cultured in medium onto gold-plated electrodes of a 96-well E-plate and for each well the impedance is measured on predefined time intervals at 10 kHz. The impedance is converted to the unitless parameter Cell Index (CI), which can be plotted over time:

$$CI = \frac{(Z_i - Z_0)\Omega}{15\Omega}$$

where Z_i is the impedance at any given time point and Z_0 is the baseline impedance measured at the start of each experiment[50].

Assays were performed at 37°C and 5% CO_2 in a final volume of 100 μl/well. Baseline impedance was measured in 40 μl culture medium prior to cell seeding. Cells grown to 70–80% confluence were seeded in 50 μl at 60,000 cells/well in the presence of 1 μg/ml dox to induce EAAT1 expression and left at RT for 30 min prior to placement of the E-plate

in the RTCA recording station. After 22 h, cells were pretreated with 5 µl vehicle (PBS/DMSO) or, in inhibitor experiments, 1 nM – 10 µM of TFB-TBOA or UCPH-101 or 1 µM ouabain, and impedance was recorded for 60 min. Subsequently, cells were stimulated with 5 µl vehicle (PBS), 10 µM – 1 mM L-glutamate (submaximal concentration [EC_{80}, 1 mM] in inhibitor experiments) or L-aspartate, 200 nM TFB-TBOA (EC_{50}) or 6.3 µM UCPH-101 (EC_{50}), and impedance was recorded for 120 min. Each condition was tested in duplicate per experiment and levels of DMSO were kept constant at 0.1% for all assays and wells.

7.4.12 – Data analysis and statistics

7.4.12.1 – Whole-cell HA-tag ELISA

In each experiment, the mean absorbance for each condition was divided over the mean absorbance of non-induced (–dox) JumpIn-$EAAT1_{WT}$ cells to obtain fold expression over –dox cells. To assess whether total protein expression of dox-induced (+dox) JumpIn-EAAT1 mutant cells was significantly different from +dox JumpIn-$EAAT1_{WT}$ cells, a one-way ANOVA with Dunnett's post-hoc test was done for cells that were tested on the same ELISA plate.

7.4.12.2 – Impedance-based phenotypic assay

Data was recorded using RTCA Software v2.0 or v2.1.1 (ACEA Biosciences). Depending on the part that was used for analysis, the CI values were normalized to the time of inhibitor pretreatment or substrate stimulation yielding normalized CI (nCI) values for all subsequent data points. The nCI values were exported and analyzed in GraphPad Prism v9 (GraphPad Software, San Diego, CA, USA). Vehicle-only conditions were subtracted from all other conditions to correct for vehicle-induced, ligand-independent effects. The remaining nCI curves were quantified by analyzing the net area under the curve (AUC) of the first 120 min after substrate stimulation. The AUC values, which are expressed as the cellular response, were fitted to a sigmoidal concentration-effect curve with a variable slope to determine the potencies of the EAAT1 substrates and inhibitors. Data are shown as the mean ± standard error of the mean (SEM) of at least three separate experiments each performed in duplicate, unless stated otherwise. Comparison of multiple mean values to a control (i.e., $EAAT1_{WT}$) was done using a one-way ANOVA with Dunnett's post-hoc test. Differences were considered statistically significant when p-values were below 0.05.

References

1. Tzingounis, A. V. & Wadiche, J. I. (2007) Glutamate transporters: confining runaway excitation by shaping synaptic transmission. *Nat. Rev. Neurosci.* **8**, 935–947.
2. Vandenberg, R. J. & Ryan, R. M. (2013) Mechanisms of glutamate transport. *Physiol. Rev.* **93**, 1621–1657.
3. Alleva, C., Machtens, J.-P., Kortzak, D., Weyand, I. & Fahlke, C. (2022) Molecular basis of coupled transport and anion conduction in excitatory amino acid transporters. *Neurochem. Res.* **47**, 9–22.
4. Peterson, A. R. & Binder, D. K. (2020) Astrocyte glutamate uptake and signaling as novel targets for antiepileptogenic therapy. *Front. Neurol.* **11**, 1006.
5. Lewerenz, J. & Maher, P. (2015) Chronic glutamate toxicity in neurodegenerative diseases–What is the evidence? *Front. Neurosci.* **9**, 1–20.
6. Yi, H., Talmon, G. & Wang, J. (2020) Glutamate in cancers: from metabolism to signaling. *J. Biomed. Res.* **34**, 260–270.
7. Freidman, N. *et al.* (2020) Amino acid transporters and exchangers from the SLC1A family: Structure, mechanism and roles in physiology and cancer. *Neurochem. Res.* **45**, 1268–1286.
8. Kortagere, S. *et al.* (2018) Identification of novel allosteric modulators of glutamate transporter EAAT2. *ACS Chem. Neurosci.* **9**, 522–534.
9. Jensen, A. A. *et al.* (2009) Discovery of the first selective inhibitor of excitatory amino acid transporter subtype 1. *J. Med. Chem.* **52**, 912–915.
10. Takano, T. *et al.* (2001) Glutamate release promotes growth of malignant gliomas. *Nat. Med.* **7**, 1010–1015.
11. Robert, S. M. & Sontheimer, H. (2014) Glutamate transporters in the biology of malignant gliomas. *Cell. Mol. Life Sci.* **71**, 1839–1854.
12. Corbetta, C. *et al.* (2019) Altered function of the glutamate–aspartate transporter GLAST, a potential therapeutic target in glioblastoma. *Int. J. Cancer* **144**, 2539–2554.
13. Garcia-Bermudez, J. *et al.* (2018) Aspartate is a limiting metabolite for cancer cell proliferation under hypoxia and in tumours. *Nat. Cell Biol.* **20**, 775–781.
14. Tajan, M. *et al.* (2018) A role for p53 in the adaptation to glutamine starvation through the expression of SLC1A3. *Cell Metab.* **28**, 721–736.
15. Bacci, M. *et al.* (2019) Reprogramming of amino acid transporters to support aspartate and glutamate dependency sustains endocrine resistance in breast cancer. *Cell Rep.* **28**, 104–118.
16. Chivukula, A. S., Suslova, M., Kortzak, D., Kovermann, P. & Fahlke, C. (2020) Functional consequences of SLC1A3 mutations associated with episodic ataxia 6. *Hum. Mutat.* **41**, 1892–1905.
17. Adamczyk, A. *et al.* (2011) Genetic and functional studies of a missense variant in a glutamate transporter, SLC1A3, in Tourette syndrome. *Psychiatr. Genet.* **21**, 90–97.
18. Kovermann, P. *et al.* (2017) Impaired K+ binding to glial glutamate transporter EAAT1 in migraine. *Sci. Rep.* **7**, 13913.
19. van Amen-Hellebrekers, C. J. M. *et al.* (2016) Duplications of SLC1A3: Associated with ADHD and autism. *Eur. J. Med. Genet.* **59**, 373–376.
20. Boudker, O., Ryan, R. M., Yernool, D., Shimamoto, K. & Gouaux, E. (2007) Coupling substrate and ion binding to extracellular gate of a sodium-dependent aspartate transporter. *Nature* **445**, 387–393.
21. Guskov, A., Jensen, S., Faustino, I., Marrink, S. J. & Slotboom, D. J. (2016) Coupled binding mechanism of three sodium ions and aspartate in the glutamate transporter homologue GltTk. *Nat. Commun.* **7**, 13420.
22. Canul-Tec, J. C. *et al.* (2017) Structure and allosteric inhibition of excitatory amino acid transporter 1. *Nature* **544**, 446–451.
23. Canul-Tec, J. C. *et al.* (2022) The ion-coupling mechanism of human excitatory amino acid transporters. *EMBO J.* **41**, e108341.
24. Kato, T. *et al.* (2021) Structural insights into human excitatory amino acid transporter EAAT2. *bioRxiv* **preprint**, 1–34.
25. Qiu, B., Matthies, D., Fortea, E., Yu, Z. & Boudker, O. (2021) Cryo-EM structures of excitatory amino acid transporter 3 visualize coupled substrate, sodium, and proton binding and transport. *Sci. Adv.* **7**, eabf5814.
26. Schaller, L. & Lauschke, V. M. (2019) The genetic landscape of the human solute carrier (SLC) transporter superfamily. *Hum. Genet.* **138**, 1359–1377.
27. Jensen, M. A., Ferretti, V., Grossman, R. L. & Staudt, L. M. (2017) The NCI Genomic Data Commons as an engine for precision medicine. *Blood* **130**, 453–459.
28. Shimamoto, K. *et al.* (2004) Characterization of novel L-threo-β-Benzyloxyaspartate derivatives, potent blockers of the glutamate transporters. *Mol. Pharmacol.* **65**, 1008–1015.
29. Cournia, Z., Allen, B. & Sherman, W. (2017) Relative binding free energy calculations in drug discovery: Recent advances and practical considerations. *J. Chem. Inf. Model.* **57**, 2911–2937.
30. Vettore, L., Westbrook, R. L. & Tennant, D. A. (2020) New aspects of amino acid metabolism in cancer. *Br. J. Cancer* **122**, 150–156.
31. Winter, N., Kovermann, P. & Fahlke, C. (2012) A point mutation associated with episodic ataxia 6 increases glutamate transporter anion currents. *Brain* **135**, 3416–3425.

32. Alleva, C. *et al.* (2020) Na +-dependent gate dynamics and electrostatic attraction ensure substrate coupling in glutamate transporters. *Sci. Adv.* **6**, eaba9854.

33. Abrahamsen, B. *et al.* (2013) Allosteric modulation of an excitatory amino acid transporter: the subtype-selective inhibitor UCPH-101 exerts sustained inhibition of EAAT1 through an intramonomeric site in the trimerization domain. *J. Neurosci.* **33**, 1068–1087.

34. Wu, Q. *et al.* (2022) Ataxia-linked SLC1A3 mutations alter EAAT1 chloride channel activity and glial regulation of CNS function. *J. Clin. Invest.* **132**, e154891.

35. Bastug, T. *et al.* (2012) Position of the third Na+ site in the aspartate transporter GltPh and the human glutamate transporter, EAAT1. *PLoS One* **7**, e33058.

36. Choi, K.-D. *et al.* (2017) Genetic variants associated with episodic ataxia in Korea. *Sci. Rep.* **7**, 13855.

37. Seal, R. P. & Amara, S. G. (1998) A reentrant loop domain in the glutamate carrier EAAT1 participates in substrate binding and translocation. *Neuron* **21**, 1487–1498.

38. Chen, I. *et al.* (2021) Glutamate transporters have a chloride channel with two hydrophobic gates. *Nature* **591**, 327–331.

39. Cater, R. J., Vandenberg, R. J. & Ryan, R. M. (2014) The domain interface of the human glutamate transporter EAAT1 mediates chloride permeation. *Biophys. J.* **107**, 621–629.

40. Trinco, G. *et al.* (2021) Kinetic mechanism of Na+-coupled aspartate transport catalyzed by GltTk. *Commun. Biol.* **4**, 751.

41. Kortzak, D. *et al.* (2019) Allosteric gate modulation confers K+ coupling in glutamate transporters. *EMBO J.* **38**, e101468.

42. Leighton, B. H., Seal, R. P., Shimamoto, K. & Amara, S. G. (2002) A hydrophobic domain in glutamate transporters forms an extracellular helix associated with the permeation pathway for substrates. *J. Biol. Chem.* **277**, 29847–29855.

43. Scopelliti, A. J., Font, J., Vandenberg, R. J., Boudker, O. & Ryan, R. M. (2018) Structural characterisation reveals insights into substrate recognition by the glutamine transporter ASCT2/SLC1A5. *Nat. Commun.* **9**, 38.

44. Levine, M. V, Cuendet, M. A., Khelashvili, G. & Weinstein, H. (2016) Allosteric mechanisms of molecular machines at the membrane: Transport by sodium-coupled symporters. *Chem. Rev.* **116**, 6552–6587.

45. Bongers, B. J. *et al.* (2021) Pan-cancer in silico analysis of somatic mutations in G-protein coupled receptors: The effect of evolutionary conservation and natural variance. *bioRxiv* **preprint**, 1–41.

46. Auton, A. *et al.* (2015) A global reference for human genetic variation. *Nature* **526**, 68–74.

47. The UniProt Consortium. (2019) UniProt: a worldwide hub of protein knowledge. *Nucleic Acids Res.* **47**, D506–D515.

48. Abagyan, R., Totrov, M. & Kuznetsov, D. (1994) ICM—A new method for protein modeling and design: Applications to docking and structure prediction from the distorted native conformation. *J. Comput. Chem.* **15**, 488–506.

49. Neves, M. A. C., Totrov, M. & Abagyan, R. (2012) Docking and scoring with ICM: The benchmarking results and strategies for improvement. *J. Comput. Aided. Mol. Des.* **26**, 675–686.

50. Kho, D. *et al.* (2015) Application of xCELLigence RTCA biosensor technology for revealing the profile and window of drug responsiveness in real time. *Biosensors* **5**, 199–222.

Supplementary Information

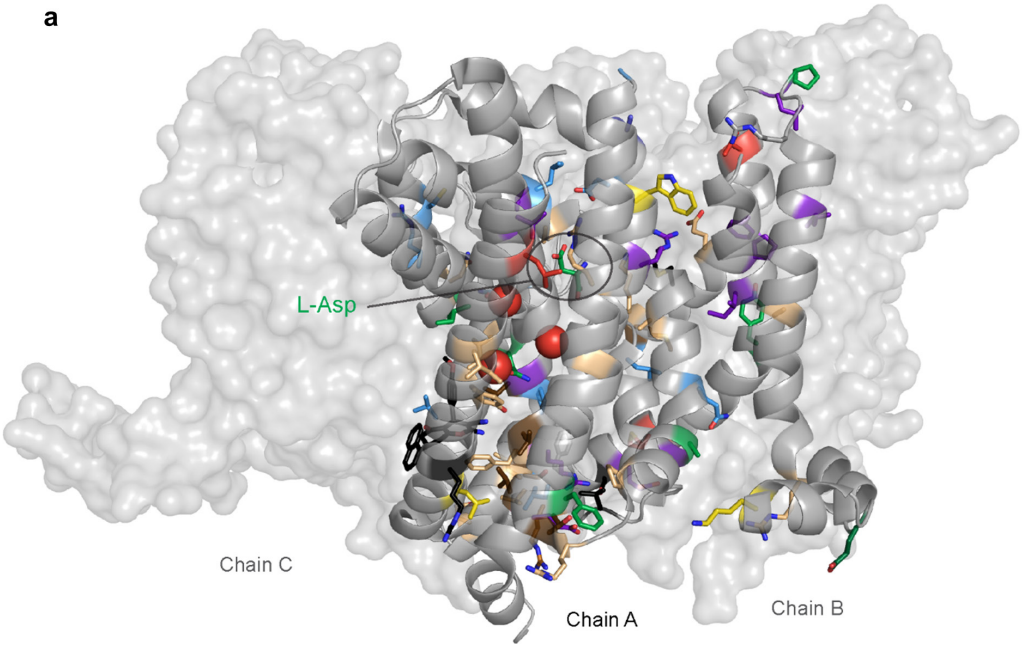

Supplementary Figure 7.S1 – Structural distribution of cancer-related mutants per cancer type. Mutations from the Genomic Data Commons mapped onto the biological assembly of EAAT1 (PDB 7AWM). Chain A is represented as a grey cartoon, while chains B and C are represented as grey surfaces. The co-crystalized substrate, L-aspartate, is represented as green sticks in chain A. The three coordinated Na^+ ions are represented as red spheres in chain A. Residues that have been observed mutated in cancer patients are colored by cancer primary site following the colors in the key. (**a**) Frontal view, as aligned with cellular membrane. (**b**) Top view, as seen from the extracellular side.

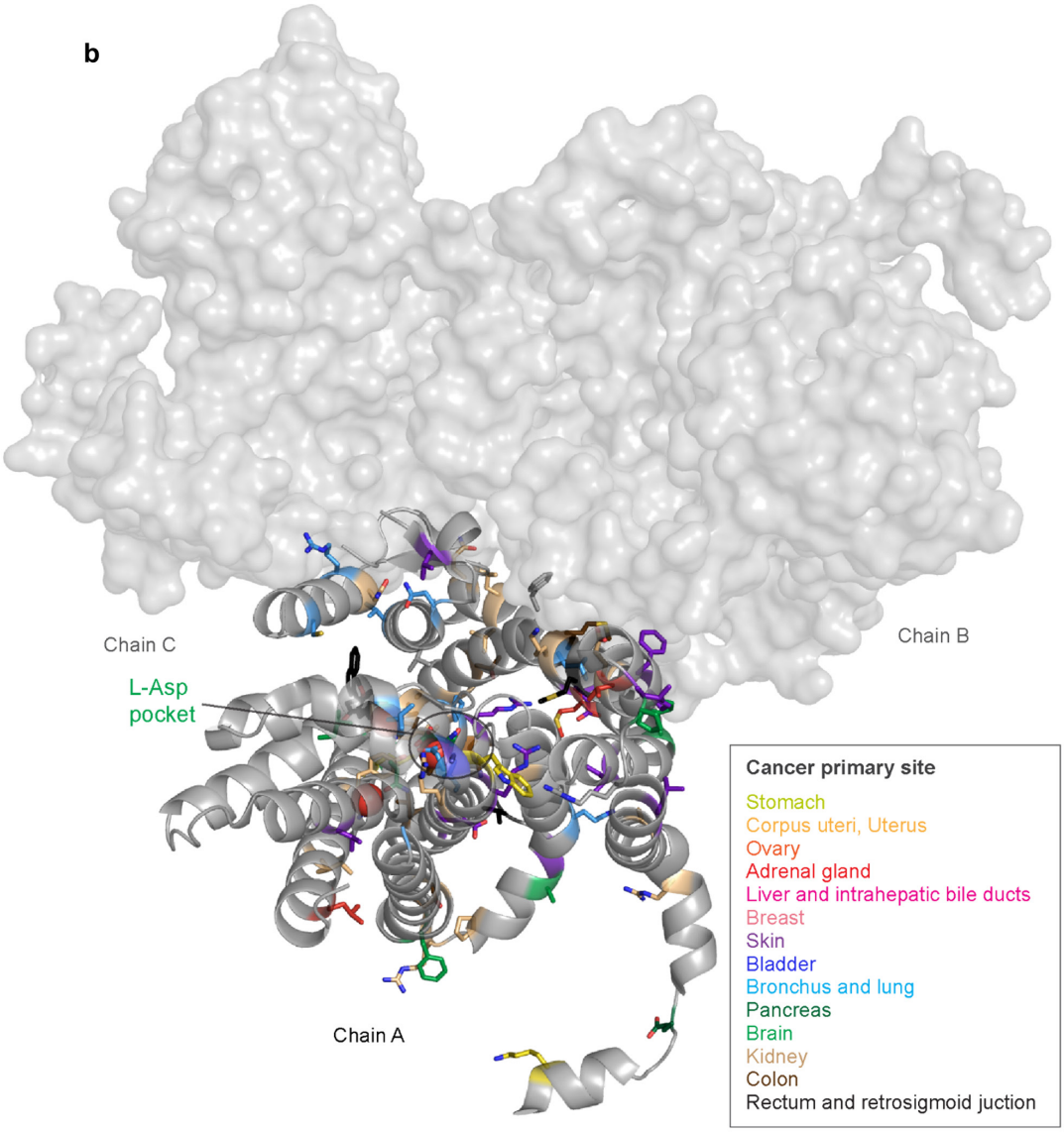
b
Chain C
Chain B
L-Asp
pocket
Chain A
Cancer primary site
Stomach
Corpus uteri, Uterus
Ovary
Adrenal gland
Liver and intrahepatic bile ducts
Breast
Skin
Bladder
Bronchus and lung
Pancreas
Brain
Kidney
Colon
Rectum and retrosigmoid juction

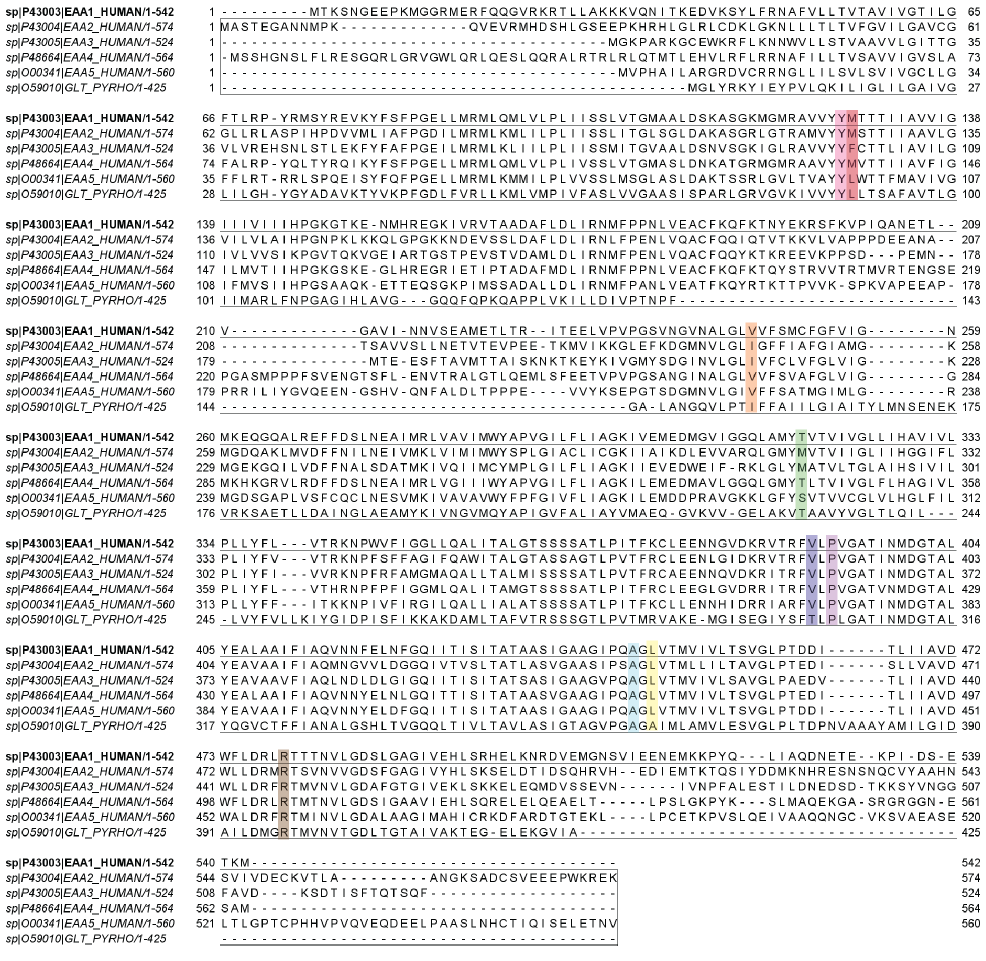

Supplementary Figure 7.S2 – Conservation of selected cancer-related mutants in EAAT family. Multiple sequence alignment of human EAATs (EAAT1–5) and *Pyrococcus horikoshii* homolog Glt_{Ph} computed in ClustalOmega. Colored, the positions of the cancer-related mutants analyzed *in vitro:* Y127C (pink), V247F (orange), V390M (dark blue), P392L (purple), A446V/E (blue), L448Q (yellow), R479W (brown). For reference, ataxia-related reference mutants are also colored: M128R (red) and T318A (green).

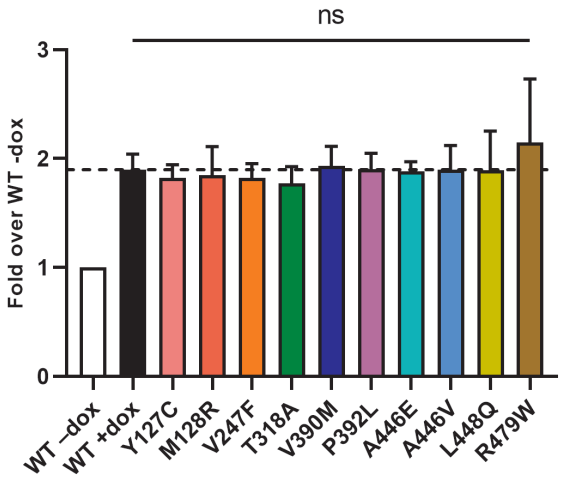

Supplementary Figure 7.S3 – Whole-cell HA-tag ELISA on $EAAT1_{WT}$ and mutant cells. Cells were grown for 24 h in the absence (–dox, WT only) or presence (+dox, WT and mutants) of 1 µg/ml doxycycline. Presence of total HA-tagged protein (plasma membrane and cytosolic) was determined in permeabilized cells. Absorbance for each condition is expressed as fold expression over WT (–dox). Data are shown as the mean ± SEM of twelve (WT), six (M128R) or three (rest) individual experiments each performed in quintuplicate. Significant differences between $EAAT1_{WT}$ and mutant cells were determined using one-way ANOVA with Dunnett's post-hoc test. ns = not significant for all mutants.

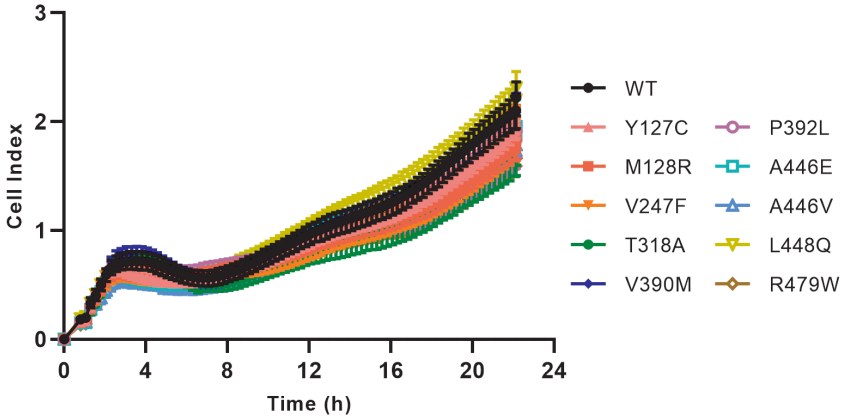

Supplementary Figure 7.S4 – Representative growth curves of $EAAT1_{WT}$ and EAAT1 mutant cells in an impedance-based phenotypic assay. Data are shown as the mean ± SD of eight replicates from a representative experiment.

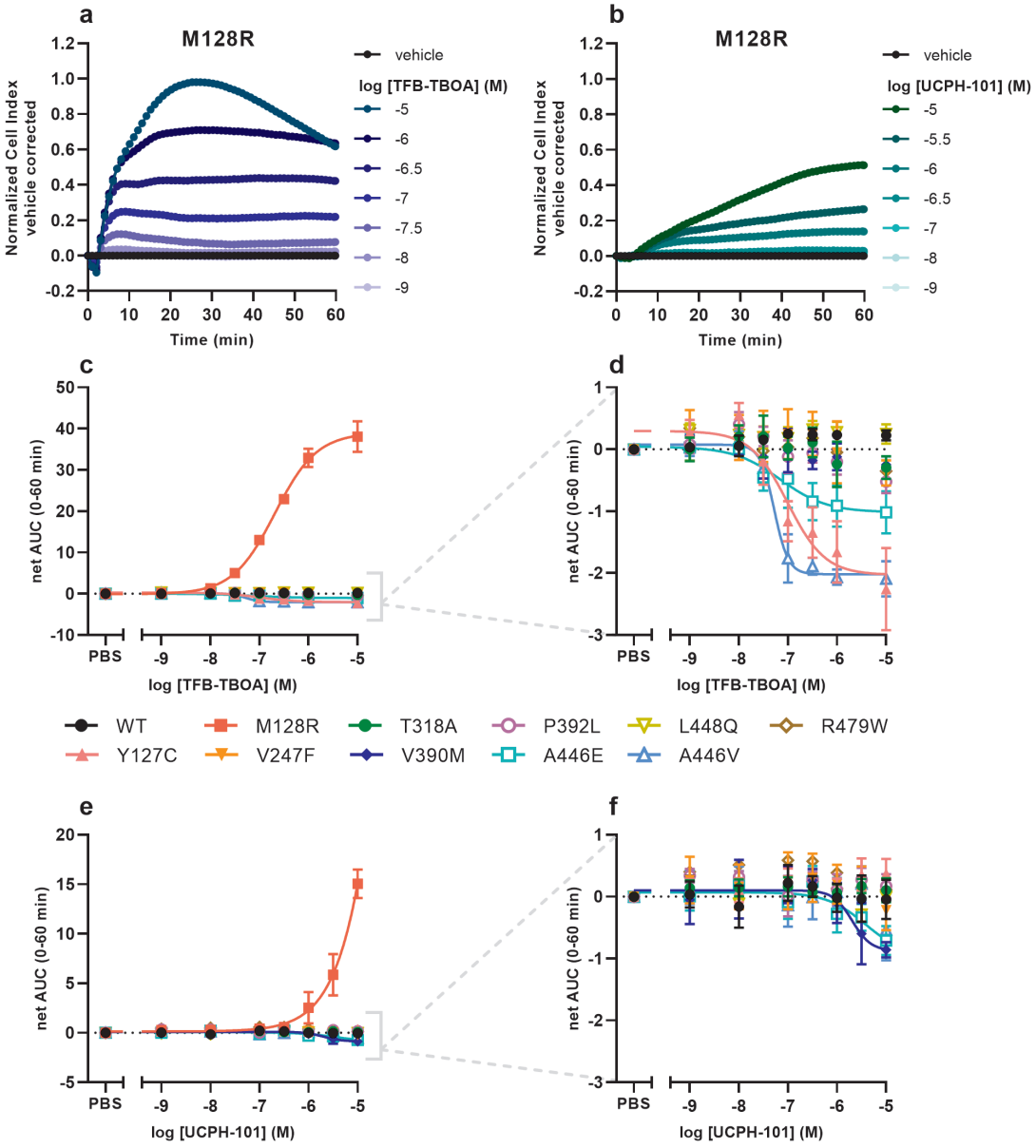

Supplementary Figure 7.S5 – Cellular responses of TFB-TBOA and UCPH-101 during pretreatment in an impedance-based phenotypic assay on $EAAT_{WT}$ and mutant cells. (**a,b**) Vehicle-corrected normalized Cell Index traces of M128R cells pretreated with (**a**) TFB-TBOA or (**b**) UCPH-101 from a representative experiment. (**c**) Concentration-response curves of TFB-TBOA on M128R cells and (**d**) zoom-in on $EAAT1_{WT}$ and other mutant cells. (**e**) Concentration-response curves of UCPH-101 on M128R cells and (**f**) zoom-in on $EAAT1_{WT}$ and other mutant cells. Cellular response is expressed as the net AUC of the first 60 min after inhibitor pretreatment. Data are shown as the mean ± SEM of three individual experiments each performed in duplicate.

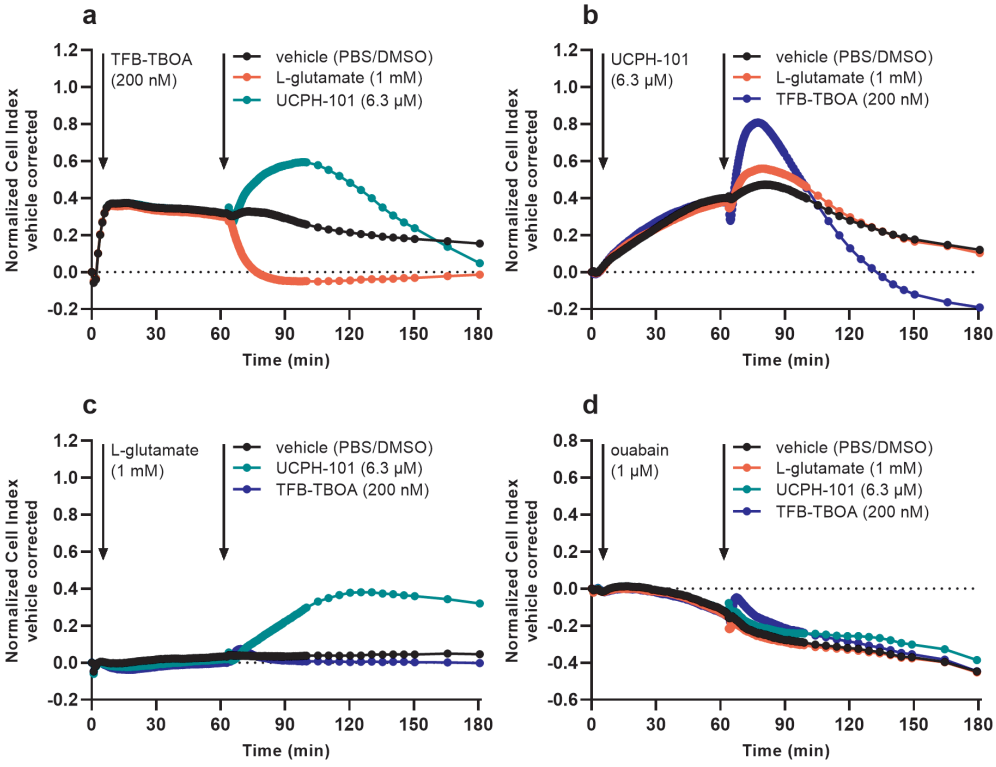

Supplementary Figure 7.S6 – Modulation of cellular responses by L-glutamate and inhibitors in an impedance-based phenotypic assay on M128R cells. (**a**) Pretreatment with EC_{50} (200 nM) TFB-TBOA and stimulation with vehicle, 1 mM L-glutamate or EC_{50} (6.3 µM) UCPH-101. (**b**) Pretreatment with 6.3 µM UCPH-101 and stimulation with vehicle, 1 mM L-glutamate or 200 nM TFB-TBOA. (**c**) Pretreatment with 1 mM L-glutamate and stimulation with vehicle, 6.3 µM UCPH-101 or 200 nM TFB-TBOA. (**d**) Pretreatment with 1 µM ouabain (Na^+/K^+-ATPase inhibitor) and stimulation with vehicle, 1 mM L-glutamate, 6.3 µM UCPH-101 or 200 nM TFB-TBOA. Data show vehicle-corrected normalized Cell Index traces of M128R cells pretreated for 60 min and subsequently stimulated for 120 min. Traces were normalized at the time point prior to pretreatment. Cells pretreated and stimulated with vehicle (PBS/DMSO) were used for vehicle-correction.